mater.scichina.com link.springer.com

Published online 4 June 2024 | https://doi.org/10.1007/s40843-024-2890-1
Sci China Mater 2024, 67(7): 2153–2160

Regulating dynamic growth pathway for constructing organic heterostructures of interchangeable microblocks and adjustable optical output

Shuai Zhao[1], Chao-Fei Xu[1], Yue Yu[1], Xing-Yu Xia[1], Lei Wang[1], Xue-Dong Wang[1*] and Liang-Sheng Liao[1,2*]

ABSTRACT **Organic heterostructures (OHs) with multi-segments exhibit unique optoelectronic properties due to the directional energy transfer between adjacent segments compared with single-component structures. Nevertheless, the OHs with a spontaneously formed substructure might not meet the practical application needs. Accordingly, constructing the building blocks (crystals X and Y) into rational configurations (such as XYX or reversed YXY patterns) at will would greatly promote the development of OHs in optics. Herein, we demonstrate sequential crystallization, combining spontaneous self-assembly and seeded stepwise self-assembly processes, to manipulate longitudinal epitaxial growth of red-emissive fluorene-7,7,8,8-tetracyanoquinodimethane (R) or near-infrared-emissive fluorene-2,3,5,6-tetrafluoro-7,7,8,8-tetracyanoquinodimethane (N) on each other, resulting in the OHs with interchangeable block patterns: RNR and NRN. The OHs with RNR pattern display gradient-color emission and waveguide property as a result of gradually-doped heterojunction, while the NRN-pattern OHs exhibit pure dual-color emission and waveguide property due to the well-defined boundary. This work realizes the order-controllable growth of blocks in OHs and affords an avenue to rationally construct complex OHs for future optics development.**

Keywords: organic heterostructure, charge transfer cocrystal, crystallization, optical waveguide

INTRODUCTION

Low-dimensional organic crystalline heterostructures (OHs) hold great potential in optoelectronics applications ranging from display [1–3] and optical waveguide [4–8] to on-chip optical computing [9,10], due to their typical spatially segmented emission properties [11,12]. Benefiting from the advantages of high chemical/structure compatibility and tunable optoelectronic properties, organic cocrystals gradually become a competitive candidate for constructing OHs with core/shell [8,13–16], branch [17,18], and multi-block [19–21] structures. Up to now, several technical methods have been developed for constructing OHs. Chandrasekar's group [22,23] utilized the atomic force microscopy (AFM) cantilever to micromechanically integrate three different flexible crystals for multiple color optical waveguide. Catalano *et al.* [24] also prepared a hybrid large-bandwidth optical waveguide by a physical combination of crystals. Hosseini's group [7,25] reported the welding of crystals by self-assembly processes for core/shell and multi-block heterostructures. Lan *et al.* [26] proposed a layer-by-layer charged polymer assembly approach to combine different crystals into hybrid organic photonic integrated circuits. Our group [27,28] prepared OHs based on lattice-matching epitaxial growth of organic charge transfer (CT) cocrystals, through which the morphology evolution of OHs can be kinetically and thermodynamically controlled [29].

In particular, the novel rectifying effect at the heterojunction for one-dimensional (1D) OHs and the quantum confinement effect have promoted it as a good candidate for optical communication [29–31]. Even though tailoring the thermodynamic and kinetic growth pathways in the self-assembly process controls the heterostructure morphology [32], synthesis of OHs with desired substructures remains challenging [33]. The donor-acceptor (D-A) interactions between electron-D and electron-A act as directing forces for assembly and dominate the growth order of building blocks [12,33,34]. For example, the epitaxial growth of one building block (crystal X) at the tips of another building block (crystal Y) results in the OHs with a specific triblock "XYX" configuration, rather than reversed "YXY" pattern [35], while they show completely different optoelectronic properties. Therefore, developing novel strategies for rationally synthesizing OHs with a required configuration is vital for enriching the OHs library and for extending its applications in photonics.

Seeded living polymerization with seed preparation and chain-growth polymerization in the same system is developed for the fabrication of triblock polymer architectures with two kinds of reversed configurations [36,37]. However, precise kinetic control of the polymerization process remains necessary in the formation of such out-of-equilibrium block copolymers. Seed-induced living growth of block-reversed heterostructure was reported by directly altering the growth sequence of each block [19]. Significantly, this block-reversed heterostructure relies on the physical vapor transport method based on a specific alloy, which limits the diversity of materials. As mentioned

[1] Jiangsu Key Laboratory for Carbon-Based Functional Materials & Devices, Institute of Functional Nano & Soft Materials (FUNSOM), Soochow University, Suzhou 215123, China
[2] Macao Institute of Materials Science and Engineering, Macau University of Science and Technology, Macau 999078, China
[*] Corresponding authors (emails: wangxuedong@suda.edu.cn (Wang XD); lsliao@suda.edu.cn (Liao LS))

above, organic CT cocrystals show high chemical/structure compatibility and tunable optoelectronic properties *via* altering D or A [38], which overcomes the main drawback in seeded stepwise self-assembly. Impelled by these research results, we aim to construct an organic heterostructure with a reversed ABA block pattern rather than a spontaneous BAB pattern *via* seeded stepwise self-assembly based on high compatibility between CT cocrystals.

Herein, we demonstrated sequential crystallization, combining spontaneous self-assembly and seeded stepwise self-assembly processes, for controlling the crystalization sequence and for constructing two OHs with interchangeable block patterns from Flu-TNCQ (**R**) and Flu-F_4TCNQ (**N**) cocrystals (Fig. 1). The typical planar aromatic π-conjugated fluorene (Flu) with strong electron-donating capacity was selected for constructing cocrystals [39]. 7,7,8,8,-Tetracyanoquinodimethane (TCNQ) and 2,3,5,6-tetrafluoro-7,7,8,8-tetracyanoquinodimethane (F_4TCNQ) were chosen as an electron-A to tune the charge transfer interaction as well as the emission property [40]. The cocrystal structures verify the high structural compatibility between **R** and **N**, benefiting the epitaxial growth. Type 1 OHs (**RNR**) were easily synthesized by spontaneous self-assembly of Flu-TNCQ and Flu-F_4TCNQ. By artificially controlling the longitudinal epitaxial growth in the order in which the precursors were added, the Type 2 OHs (**NRN**) were also successfully synthesized with a reversed configuration compared with Type 1. Furthermore, the unique configurations of these two OHs with interchangeable block patterns display gradient- and dual-color emission or waveguide properties, giving rise to manipulating the photon behavior as well as the output signal, which expands the application of OHs in future fundamental organic optics.

EXPERIMENTAL SECTION

Materials

Flu, TCNQ and F_4TCNQ were all purchased from commercial sources and used directly without further treatment. Dichloromethane (DCM, HPLC grade) and ethanol (EtOH, HPLC grade) were purchased from Beijing Chemical Agent Ltd.

Preparations

As illustrated in Fig. S1a, the solution (100 μL) of Flu (5 mM) and electron-A (TCNQ or F_4TCNQ, 5 mM) in DCM was injected into EtOH (200 μL). Then the mixed solution was directly dropped onto the quartz substrate at room temperature in the air, and the 1D single-crystal microrods were obtained after the solvent evaporated totally.

As illustrated in Fig. S1b, the solution (100 μL) of Flu-TCNQ-F_4TCNQ (2:1:1 *n*/*n*/*n*, 5 mM for Flu) in DCM was injected into EtOH (200 μL). Then the mixed solution was directly dropped

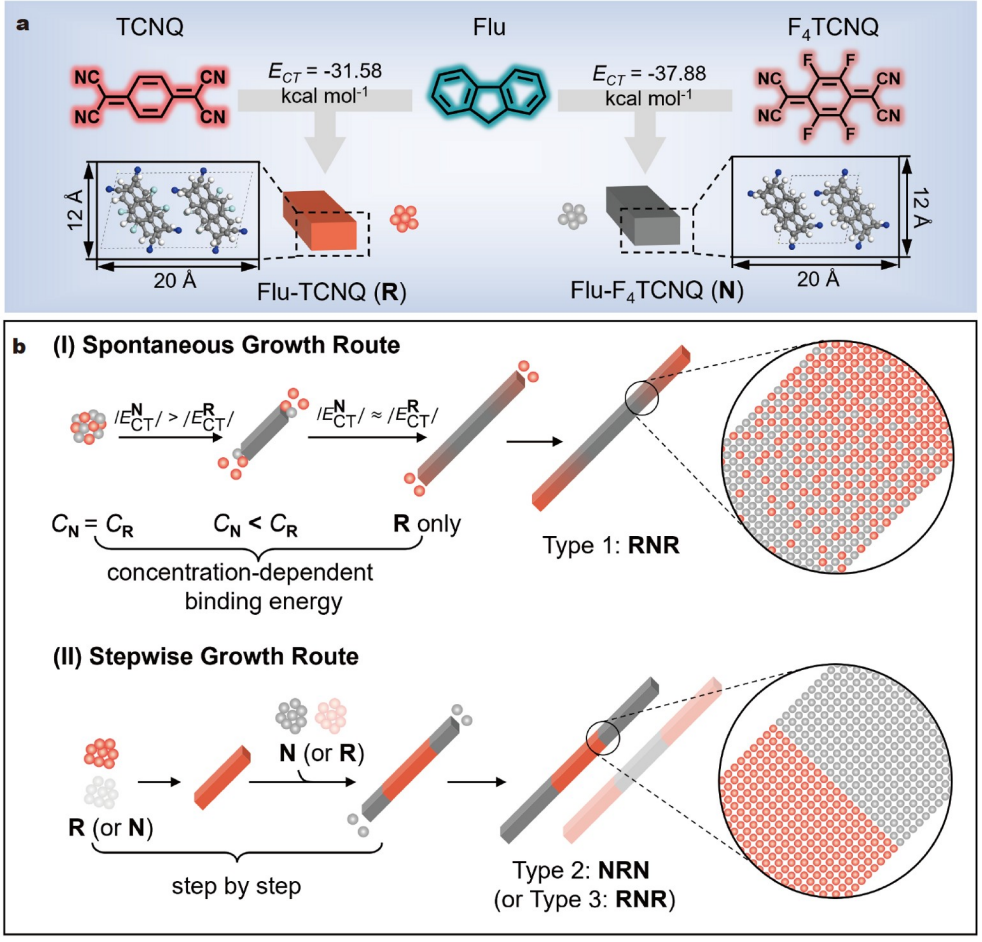

Figure 1 Growth concept of the fabrication of block-reversed OHs. (a) Schematic diagram of Flu-based cocrystals. (b) Growth strategy for three types of OHs.

onto the quartz substrate at room temperature in the air, and the Type 1 **RNR** OHs were obtained after the solvent evaporated totally.

Firstly, Flu-TCNQ (1:1 *n*/*n*) or Flu-F_4TCNQ (1:1 *n*/*n*) were dissolved in DCM and the solution (100 μL) was injected into EtOH (200 μL), respectively. Then, the solution (100 μL) of Flu-TCNQ in mixed DCM and EtOH was directly dropped onto the quartz substrate at room temperature in the air for preparing **R** seeds. After 30 s evaporation of Flu-TCNQ solution, the solution (100 μL) of F_4Flu-TCNQ in mixed DCM and EtOH was dropped onto the quartz substrate, and the Type 2 **NRN** OHs were obtained after the solvent evaporated totally.

Characterization

Fluorescence images were recorded using a fluorescence optical microscope (Leica, DM4000M, Germany) with a spot-enhanced charge couple device (Diagnostic Instrument, Inc.). X-ray diffraction experiments were carried out on a D/max 2400 X-ray diffractometer with copper (Kα) radiation (λ1.5406 Å). Transmission electron microscope (TEM) measurement was performed at room temperature with an accelerating voltage of 100 kV. Microscopic photoluminescence measurements were carried out using a homemade confocal microscopy system (Fig. S12). A 532-nm CW laser was passed through an x50 objective lens set on an optical microscope and focused onto a specimen. The PL emitted from the specimen was collected with the identical objective lens and detected with a spectrometer (Princeton Instrument, ARCSP-2356) through an optical fiber. All calculations were performed with the periodic density functional theory method using Dmol3 module in Material Studio software package.

RESULTS AND DISCUSSION

The optical microscopy (OM) and fluorescence microscopy (FM) images demonstrate that 1D microwire cocrystals **R** and **N** are successfully synthesized using a previously reported procedure [41] (Figs S1a and S2). Combined with the photoluminescence (PL) spectrum (Fig. S2c), it can be concluded that **R** and **N** display red emission and near infrared (NIR) emissions with the PL peaks at 704 and 805 nm, respectively. The emission shift from the red region to the NIR region means an enhanced CT degree for Flu-F_4TCNQ D-A pairs [42]. The XRD patterns (Fig. S3) and single crystal analysis (Figs S4, S5, and Table S1) indicate Flu and the corresponding A aggregate along [100] direction to form 1D cocrystal with high crystallinity. Fig. 1 shows the growth concept of the fabrication of block-reversed OHs. Red-emissive cocrystals Flu-TCNQ (**R**) and NIR-emissive cocrystals Flu-F_4TCNQ (**N**) were prepared firstly based on efficient CT interaction. Then, due to the structurally similar molecular arrangement between these cocrystals, the OHs (Type 1: **RNR** and Type 2: **NRN**) with reversed block order are fabricated through two strategies (Fig. 1b). When mixed thoroughly, **N** and **R** tend to form gradually-doped block Type 1 OHs as a result of their spontaneous epitaxial growth during solvent evaporation. Reversed well-defined block OHs Type 2 were fabricated *via* the self-assembly of **N** block following the crystallization of **R** seed.

Type 1 RNR OHs

Gradually doped block heterostructure was constructed through a spontaneous self-assembly method by directly evaporating the solution of Flu-TCNQ-F_4TCNQ with a molar ratio of 2:1:1. (Fig. 2a and Fig. S1b). The self-assembly process of the gradually-changed block heterostructure is dynamic and undergoes a successive crystallization of **N** to **R** blocks during solvent evaporation. The binding energy induced by CT interaction is calculated using Dmol3 module to be −37.88 and −31.58 kJ mol^{-1} for **N** and **R**, respectively, which dominates the crystallization sequence when forming block heterostructure. At the first stage of solvent evaporation, Flu-F_4TCNQ self-assembles into 1D micro-block **N** as a result of relatively strong CT interaction. After a period of self-assembly of **N**, the relative concentration of the F_4TCNQ decreases and the interaction between Flu and F_4TCNQ becomes weaker due to decreased concentration [43]. Due to the lack of F_4TCNQ during the formation of **N**, Flu-TCNQ starts to participate in the self-assembly process forming a gradually-doped structure with gradient composition of **N** and **R**. Further evaporation results in the formation of micro-block **R** at the tips of **N** micro-blocks and finally gradually-doped Type 1 block OHs. The OM and FM images (Fig. 2b and Fig. S6) indicate the Type 1 block OHs with a gradient composition between the middle **N** microcrystal and the end **R** microcrystal are fabricated successfully [44].

The TEM image (Fig. 2c) indicates that the Type 1 block OHs feature a smooth surface. The selected area electron diffraction (SAED) patterns of the blue line marked part (middle position) and the red line marked part (end position) indicate cocrystal **N** and **R** microblocks sequentially grow along the same direction of [200], forming Type 1 block OHs with high crystallinity. In particular, **R** and **N** display similar face-to-face aggregation with interplanar spacings $d_{(100)}$ of 6.52 and 6.35 Å for **R** and **N** (Fig. 2d), respectively, which results in a low lattice mismatch ratio of 2.68% and induces the continuous epitaxial growth process for constructing 1D block OHs [45]. The relative higher lattice mismatch ratio along [010] of 2.68% and along [001] results in the formation of 1D block OHs instead of core-shell structure or any other heterotructure. Moreover, the XRD patterns collected from the prepared Type 1 block OHs (Fig. S3) present a widen representative pattern as those of the individual **R** and **N** microwires, which indicates gradually-doping **R** in **N** cocrystal and the formation of gradient composition.

The line scan PL spectrum profile of a single Type 1 microwire was tested to further confirm the specific gradient composition in the block OHs (Fig. 2e–f). The detailed spectra recorded at 5 typical points from the end to the middle block are shown in Fig. 2g. Fig. 2f–g illustrates the middle (line 5) and end blocks (line 1) of Type 1 OHs respectively corresponding to **N** and **R** cocrystals. Significantly, the emission peaks continuously shift among the red and NIR regions as moving the detect point across the heterojunction approximately within 6 μm (Fig. 2f). The emission peak at the NIR region gradually shifts from 805 to 760 nm (Fig. 2g), indicating a gradient CT degree as a result of gradually doping **R** in **N** cocrystals during self-assembly [46].

Type 2 NRN OHs

The seeded stepwise growth method was utilized for artificially constructing Type 2 OHs with the block order opposite from the spontaneous self-assembly sequence. As illustrated in Fig. 3a and Fig. S1c, Type 2 OHs were fabricated through the 1st-step growth of **R** block seeds immediately followed by the 2nd-step growth of **N** blocks. In detail, after 30 s evaporation of Flu-TCNQ solution, additional Flu-F_4TCNQ solution was added to the system to

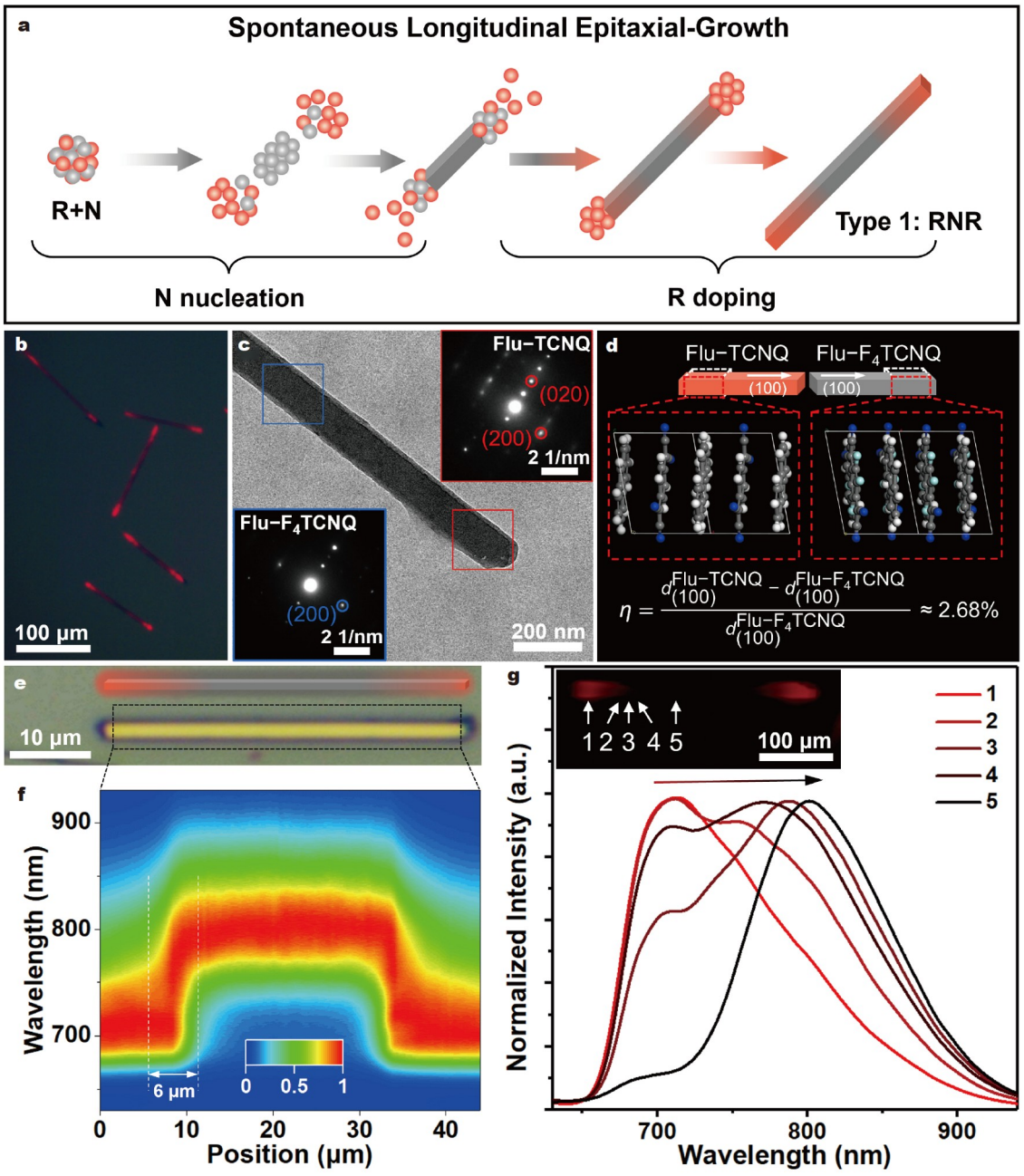

Figure 2 (a) The spontaneous longitudinal epitaxial-growth mode for the Type 1 block OHs. (b) The FM images of Type 1 block OHs. (c) The TEM image of a typical Type 1 block OH. Inset: SAED patterns of Type 1 block OH recorded at the middle (Flu-F_4TCNQ, marked with blue) and end tip (Flu-TCNQ, marked with red). (d) Molecular arrangement and orientation of heterostructure building blocks. (e) The OM image of one typical organic triple-block microwire. (f) The line scan spectrum profile of the single Type 1 block OH marked in (e). (g) The spatially resolved PL spectra corresponding to different locations of Type 1 block OH marked in the inserted FM images.

achieve continuous growth of heterostructure building blocks. The pre-existing **R** microblocks acted as seeds for the further epitaxial growth of **N**, forming the Type 2 OHs with clear boundaries. The OM and FM images marked with dashed lines indicate the middle and end blocks correspond to the **N** and **R** crystals. The line scan PL spectra profile of a single Type 2 microwire was also recorded (Fig. 3d, e and Fig. S7). Type 2 shows a dramatic emission shift from the red to NIR region within a short length of less than 1 μm at the heterojunction between **R** and **N** blocks. The spectra recorded at the heterojunction include the characteristic peaks as those of middle and end block parts, indicating direct epitaxial growth of Flu-F_4TCNQ at the end tips of Flu-TCNQ microwires without doping. Different from the gradient emission property at the heterojunction of gradually-doped Type 1 OHs, well-defined Type 2 OHs display pure dual-color emission. The well-defined Type 3 OHs with **N** microwires as middle and **R** microwires as end tips were also fabricated successfully through the 2-steps seeded growth method (Fig. 1b and Fig. S8), which means the stepwise growth method is key in the formation of a keen interface.

The difference in epitaxial growth for Type 1 and Type 2 OHs

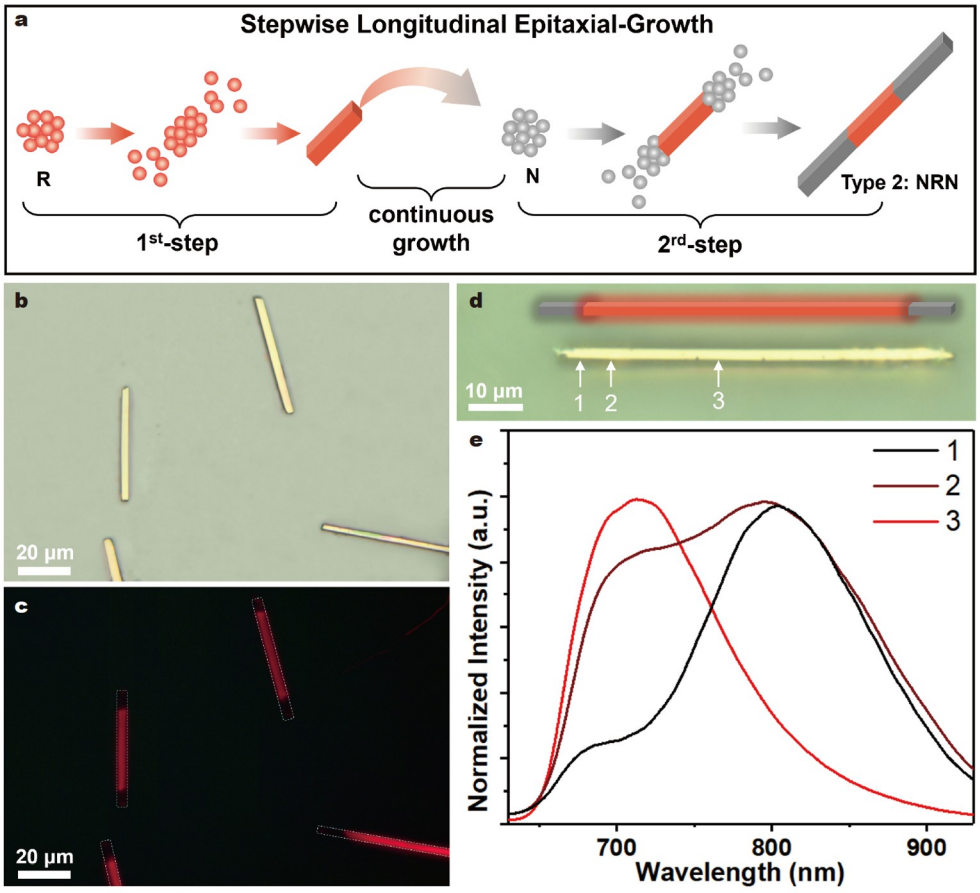

Figure 3 (a) The stepwise seeded longitudinal epitaxial-growth mode for the organic multiblock heterostructure Type 2. (b, c) The FM and OM images of Type 2 block OHs. (d) FM image of one typical organic triple-block microwire. (e) The spatially resolved PL spectra corresponding to different locations marked in (d).

was analyzed by dynamically recording the block growth during precursor evaporation and calculating the length ratio ($\eta_L = L_2$:L_1) (Fig. 4a, b and Fig. S9). It can be seen in Fig. S9, direct evaporation of Flu-TCNQ-F_4TCNQ precursor induces the successive crystallization of **N** and **R**, resulting in Type 1 heterostructure. On the contrary, after pouring the precursor of **R** on the pre-generated **N** blocks, the **R** blocks grow and lengthen gradually at the end tips of **N** microwires, eventually forming the Type 2 heterostructure (Fig. 4a). The η_L increased from 0.34 to 1.27 within a short period of 4 s (Fig. 4b). Moreover, the molar ratio ($\eta_m = n_N$:n_R) of Flu-TCNQ and Flu-F_4TCNQ in precursors for self-assembly is adjusted for finely controlling the length ratio in OHs (Fig. 4c–f, and Figs S10, S11). An obvious elongation of **N** blocks appears after increasing η_m from 0.5:1 to 3:1 for Type 2 heterostructure (Fig. 4c–f). Notably, the **R** microwires become thin and short due to the low concentration for the η_m of 3:1, resulting in a thin and unregular triblock heterostructure. Likewise, the length ratio between **N** part and **R** part of Type 1 OHs illustrates considerable enhancement with the increased η_m from 0.5:1 to 3:1 (Fig. 4h and Fig. S10). It is concluded from these results that the length ratio for OHs mentioned above can be artificially modulated by simply tuning their concentration ratio in the precursor.

Optical logic operation

Organic OHs have been widely explored for fundamental photonic applications due to the unique charge and energy transfer at the heterojunction [31]. Therefore, photon propagation behaviors in block-reversed Type 1 OHs of gradient-color emission and Type 2 OHs of dual-color emission were further investigated by recording the PL spectra at one tip while moving the excitation position along the longitudinal axis (Fig. 5 and Fig. S11). When the input laser focuses on the top **R** block of Type 1 (Fig. 5b), the emitted red light propagates along the heterostructure and undergoes energy transfer at the graded heterojunction [47], resulting in the broad emission PL output (Fig. 5d, lines 1–3). With moving the excitation position, the PL spectra recorded at the bottom end show a gradual shift profile from the red region (lines 1 and 2) to the NIR region (lines 3–8) and finally back to the red region (lines 9 and 10) due to the symmetrical gradient composition, which contributes to the gradient-color waveguide of Type 1. This unique gradient-color waveguide, PL profile at the end tip gradually shifting along with moving excitation point, can be regarded as an optical "slide rheostat" for precisely modulating the output signal in organic photonics. Nevertheless, Type 2 shows a dual-color waveguide from the characteristic PL emission of **N** and **R** blocks (Fig. 5h). When the input laser focuses on the **N** block, the emitted NIR light propagates through the heterostructure and shows monochromatic emission output with a PL peak of 805 nm at the end tip (lines 11 and 20). The energy transfer still exists between the middle **R** block and the right **N** blocks for emitted red light from

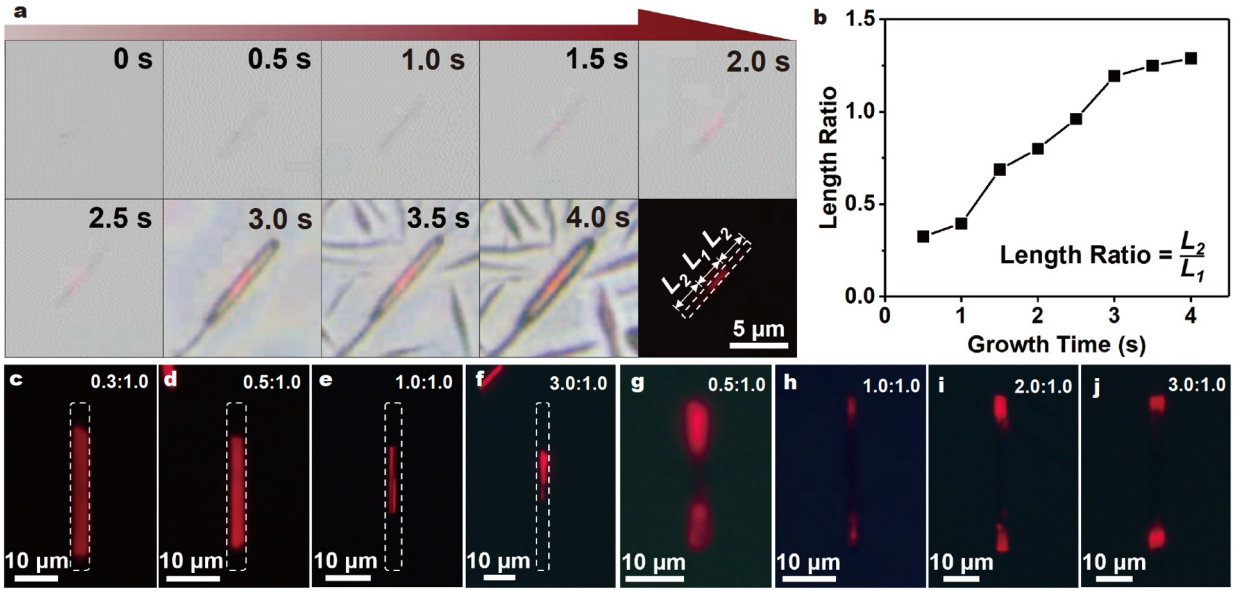

Figure 4 (a) Time-resolved growth process images of Type 2 OHs. (b) The diagram of length ratio *versus* growth time corresponds to Type 2 OHs in (a). (c–f) FM images of Type 2 OHs prepared with varied concentration ratios (η_{c2}). (g–j) FM images of Type 1 OHs prepared with varied concentration ratios (η_{c1}).

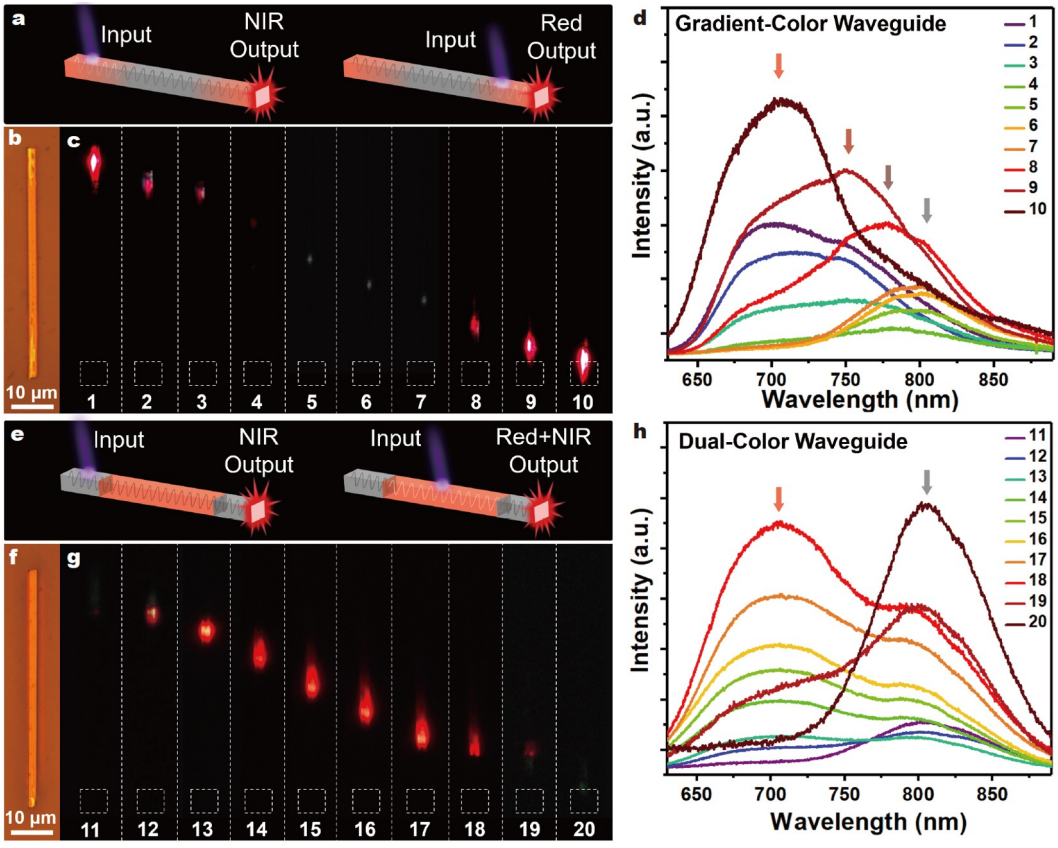

Figure 5 (a) Schematic diagram of spatially controlled optical logic operation on organic Type 1 OHs. (b) The OM image of a typical Type 1 OH. (c) The FM images of a typical Type 1 OH in (b) upon excitation from top tip to bot tip. (d) Spatially resolved PL spectra collected from bot tips marked in FM images for Type 1 OHs in (c). (e) Schematic diagram of spatially controlled optical logic operation on organic Type 2 OHs. (f) The OM image of a typical Type 2 OH. (g) The FM images of a typical Type 2 OH in (f) upon excitation from top tip to bot tip. (h) Spatially resolved PL spectra collected from bot tips marked in FM images for Type 1 OHs in (g).

the **R** block, contributing to the dual-color emission output at the end tip (Fig. 5d, lines 12–19). Therefore, these Type 1 and Type 2 OHs exhibit distinctive gradient-color waveguides and dual-color waveguides, respectively, demonstrating a great

advantage in modulating the generation and propagation of light among the visible red region and NIR region.

CONCLUSIONS

In summary, Type 1 and Type 2 OHs with totally-reversed block order were successfully fabricated *via* sequential crystallization of each block modulating the epitaxial-growth approach. Firstly, spontaneous epitaxial growth was used to construct heterostructure Type 1 with gradually-doped heterojunction based on a similar lattice structure and binding energy. Then the block order was artificially regulated through seeded stepwise self-assembly strategies for constructing well-defined heterostructure Type 2. By tuning the concentration of the species in precursor, the length ratio of organic OHs was precisely controlled. Furthermore, owing to their unique structure, these as-prepared OHs Type 1 and Type 2 display particular gradient-color waveguides and dual-color waveguides respectively, serving as efficient manipulation of optical output. This work opens up a new insight into the rational design and the synthesis of OHs with desired spatial configuration for precisely controlling the photon behavior in future photonics devices.

Received 8 February 2024; accepted 20 March 2024; published online 4 June 2024

1 Zhou Z, Zhao J, Du Y, *et al.* Organic printed core–shell heterostructure arrays: a universal approach to all-color laser display panels. Angew Chem Int Ed, 2020, 59: 11814–11818
2 Lv Y, Li YJ, Li J, *et al.* All-color subwavelength output of organic flexible microlasers. J Am Chem Soc, 2017, 139: 11329–11332
3 Wang J, Xu S, Zhang H, *et al.* Surface-doped organic charge transfer cocrystal heterostructures and their variable dual-color light emission and propagation. Cryst Growth Des, 2021, 21: 2699–2710
4 Tian D, Chen Y. Optical waveguides in organic crystals of polycyclic arenes. Adv Opt Mater, 2021, 9: 2002264
5 Venkatakrishnarao D, Mohiddon MA, Chandrasekhar N, *et al.* Waveguides: photonic microrods composed of photoswitchable molecules: erasable heterostructure waveguides for tunable optical modulation. Adv Opt Mater, 2015, 3: 1034
6 Awad WM, Davies DW, Kitagawa D, *et al.* Mechanical properties and peculiarities of molecular crystals. Chem Soc Rev, 2023, 52: 3098–3169
7 Catalano L, Berthaud J, Dushaq G, *et al.* Sequencing and welding of molecular single-crystal optical waveguides. Adv Funct Mater, 2020, 30: 2003443
8 Zhuo MP, Su Y, Qu YK, *et al.* Hierarchical self-assembly of organic core/multi-shell microwires for trichromatic white-light sources. Adv Mater, 2021, 33: 2102719
9 Xu CF, Yang WY, Lv Q, *et al.* Directed self-assembly of organic crystals into chip-like heterostructures for signal processing. Sci China Mater, 2023, 66: 733–739
10 Liu X, Wang K, Chang Z, *et al.* Engineering donor–acceptor heterostructure metal–organic framework crystals for photonic logic computation. Angew Chem Int Ed, 2019, 58: 13890–13896
11 Gao Z, Xu B, Zhang T, *et al.* Spatially responsive multicolor lanthanide-MOF heterostructures for covert photonic barcodes. Angew Chem Int Ed, 2020, 59: 19060–19064
12 Yang S, Feng X, Xu B, *et al.* Directional self-assembly of facet-aligned organic hierarchical super-heterostructures for spatially resolved photonic barcodes. ACS Nano, 2023, 17: 6341–6349
13 Lin H, Ma Y, Chen S, *et al.* Hierarchical integration of organic core/shell microwires for advanced photonics. Angew Chem Int Ed, 2023, 62: e202214214
14 Zhang H, Lei Y, Wang H, *et al.* Supramolecular core–shell heterostructures with controllable multi-color-emitting properties. J Mater Chem C, 2020, 8: 2669–2675
15 Yang X, Lan L, Li L, *et al.* Remote and precise control over morphology and motion of organic crystals by using magnetic field. Nat Commun, 2022, 13: 2322
16 Zhang F, Adolf CRR, Zigon N, *et al.* Molecular tectonics: hierarchical organization of heterobimetallic coordination networks into heterotrimetallic core–shell crystals. Chem Commun, 2017, 53: 3587–3590
17 Sun Y, Lei Y, Hu W, *et al.* Epitaxial growth of nanorod meshes from luminescent organic cocrystals *via* crystal transformation. J Am Chem Soc, 2020, 142: 7265–7269
18 Shi Y, Lv Q, Tao Y, *et al.* Design and growth of branched organic crystals: recent advances and future applications. Angew Chem Int Ed, 2022, 61: e202208768
19 Hai T, Feng Z, Sun Y, *et al.* Vapor-phase living assembly of π-conjugated organic semiconductors. ACS Nano, 2022, 16: 3290–3299
20 Chen Y, Jing B, Li J, *et al.* Four strategies towards customized rainbow/white light emission from a series of organic charge-transfer cocrystals and their heterostructures. Mater Chem Front, 2022, 6: 1874–1881
21 Zhang B, Xu J, Li C-, *et al.* Facile tuned TSCT-TADF in donor-acceptor MOF for highly adjustable photonic modules based on heterostructures crystals. Angew Chem Int Ed, 2023, 62: e202303262
22 Kumar AV, Godumala M, Ravi J, *et al.* A broadband, multiplexed-visible-light-transport in composite flexible-organic-crystal waveguide. Angew Chem Int Ed, 2022, 61: e202212382
23 Chandrasekar R. Mechanophotonics–a guide to integrating microcrystals toward monolithic and hybrid all-organic photonic circuits. Chem Commun, 2022, 58: 3415–3428
24 Catalano L, Commins P, Schramm S, *et al.* A filled organic crystal as a hybrid large-bandwidth optical waveguide. Chem Commun, 2019, 55: 4921–4924
25 Adolf CRR, Ferlay S, Kyritsakas N, *et al.* Welding molecular crystals. J Am Chem Soc, 2015, 137: 15390–15393
26 Lan L, Li L, Yang X, *et al.* Repair and splicing of centimeter-size organic crystalline optical waveguides. Adv Funct Mater, 2023, 33: 2211760
27 Wu B, Fan JZ, Han JY, *et al.* Dynamic epitaxial growth of organic heterostructures for polarized exciton conversion. Adv Mater, 2023, 35: 2206272
28 Su Y, Wu B, Chen S, *et al.* Organic branched heterostructures with optical interconnects for photonic barcodes. Angew Chem Int Ed, 2022, 61: e202117857
29 Soltani A, Ouerghi F, AbdelMalek F, *et al.* Comparative study of one-dimensional photonic crystal heterostructure doped with a high and low-transition temperature superconducting for a low-temperature sensor. Optics Commun, 2019, 445: 268–272
30 Qin JK, Wang C, Zhen L, *et al.* Van der Waals heterostructures with one-dimensional atomic crystals. Prog Mater Sci, 2021, 122: 100856
31 Chen J, Ouyang W, Yang W, *et al.* Recent progress of heterojunction ultraviolet photodetectors: materials, integrations, and applications. Adv Funct Mater, 2020, 30: 1909909
32 Bai L, Wang N, Li Y. Controlled growth and self-assembly of multiscale organic semiconductor. Adv Mater, 2022, 34: 2102811
33 Liu XT, Qian BB, Zhang T, *et al.* Programmable assembly of multiple donor-acceptor systems in metal-organic framework for heterogeneity manipulation and functions integration. Matter, 2022, 5: 2918–2932
34 Ma YX, Yang J, Chen SH, *et al.* Organic low-dimensional heterojunctions toward future applications. Matter, 2022, 5: 3706–3739
35 Zhuo MP, He GP, Yuan Y, *et al.* Super-stacking self-assembly of organic topological heterostructures. CCS Chem, 2021, 3: 413–424
36 Song S, Liu X, Nikbin E, *et al.* Uniform 1D micelles and patchy & block comicelles via scalable, one-step crystallization-driven block copolymer self-assembly. J Am Chem Soc, 2021, 143: 6266–6280
37 Wagner W, Wehner M, Stepanenko V, *et al.* Supramolecular block copolymers by seeded living polymerization of perylene bisimides. J Am Chem Soc, 2019, 141: 12044–12054
38 Sun L, Wang Y, Yang F, *et al.* Cocrystal engineering: a collaborative strategy toward functional materials. Adv Mater, 2019, 31: 1902328
39 Hu T, Feng X, Yang Z, *et al.* Design of scalable metalens array for optical addressing. Front Optoelectron, 2022, 15: 21
40 Huang Y, Wang Z, Chen Z, *et al.* Organic cocrystals: beyond electrical conductivities and field-effect transistors (FETs). Angew Chem Int Ed, 2019, 58: 9696–9711

41 Su Y, Yao ZF, Wu B, *et al.* Organic polymorph-based alloys for continuous regulation of emission colors. Matter, 2022, 5: 1520–1531
42 Ding Z, Shang H, Zhang S, *et al.* Insight from molecular packing: charge transfer and emission modulation through cocrystal strategies. Cryst Growth Des, 2020, 20: 5203–5210
43 Guo Y, Xu L, Liu H, *et al.* Self-assembly of functional molecules into 1D crystalline nanostructures. Adv Mater, 2015, 27: 985–1013
44 Liao X, Xie W, Han Z, *et al.* NIR photodetectors with highly efficient detectivity enabled by 2D fluorinated dithienopicenocarbazole-based ultra-narrow bandgap acceptors. Adv Funct Mater, 2022, 32: 2202364
45 Yao Y, Gao Z, Lv Y, *et al.* Heteroepitaxial growth of multiblock Ln-MOF microrods for photonic barcodes. Angew Chem Int Ed, 2019, 58: 13803–13807
46 Wang Y, Wu H, Hu W, *et al.* Color-tunable supramolecular luminescent materials. Adv Mater, 2022, 34: 2105405
47 Pham PV, Bodepudi SC, Shehzad K, *et al.* 2D heterostructures for ubiquitous electronics and optoelectronics: principles, opportunities, and challenges. Chem Rev, 2022, 122: 6514–6613

Acknowledgements The authors acknowledge the financial support from the National Natural Science Foundation of China (52173177, 21971185, and 52203234), the Natural Science Foundation of Jiangsu Province (BK20221362), the Science and Technology Support Program of Jiangsu Province (TJ-2022-002), and Jiangsu Funding Program for Excellent Postdoctoral Talent (2023ZB580). Furthermore, this work was supported by Suzhou Key Laboratory of Functional Nano & Soft Materials, Jiangsu Key Laboratory for Carbon-Based Functional Materials & Devices, Soochow University (KJS2156), Collaborative Innovation Center of Suzhou Nano Science & Technology, the 111 Project, Priority Academic Program Development of Jiangsu Higher Education Institutions (PAPD), Joint International Research Laboratory of Carbon Based Functional Materials and Devices, and Soochow University Tang Scholar. The authors acknowledge the Shiyanjia Lab (www.shiyanjia.com) for single crystal data analysis.

Author contributions Zhao S proposed the idea and wrote the paper under the guidance from Wang XD and Liao LS; Zhao S, Xu CF, Yu Y, Xia XY, and Wang L performed the experiments; all authors contributed to the general discussion.

Conflict of interest The authors declare that they have no conflict of interest.

Supplementary information Experimental details and supporting data are available in the online version of the paper.

Shuai Zhao received his PhD degree from the University of Tsukuba in 2022. Now, he is working as a postdoctoral fellow at the Institute of Functional Nano & Soft Materials (FUNSOM), Soochow University. His current research interest is about organic low-dimensional multiblock heterostructures and their optoelectronic applications.

Xue-Dong Wang is a full professor at FUNSOM, Soochow University. He received his Bachelor's degree in chemistry from Lanzhou University in 2011 and his PhD in physical chemistry from the Institute of Chemistry, Chinese Academy of Sciences (ICCAS) in 2016. His research focuses on the fine synthesis of organic micro/nanocrystals and the organic photonics including organic solid-state lasers and optical waveguides.

Liang-Sheng Liao received his Bachelor degree in physics from Nanchang University in 1982. He received his Master's degree and Doctor's degree in physics from Nanjing University in 1988 and 1996, respectively. Now, he is a full professor at FUNSOM, Soochow University. His current research focuses on organic fluorescent materials and devices, and organic micro-nano crystalline photonics materials and devices.

调控动态生长过程以构筑嵌段可换和光谱可调的有机异质结构

赵帅[1], 许超飞[1], 余悦[1], 夏星宇[1], 王磊[1], 王雪东[1*], 廖良生[1,2*]

摘要 与单一结构相比, 有机嵌段异质结构具有特殊的光电性能. 然而, 有机分子间的相互作用主导了异质结构构建单元的生长顺序, 如有机单元A、B会自发形成BAB型结构而不是相反的ABA型结构, 不能可控生长. 在此, 我们提出了次序结晶工程, 结合晶种逐步自组装, 控制共晶R与共晶N在彼此的两端纵向外延生长, 从而精确合成具有可逆嵌段构型的有机嵌段异质结构: RNR和NRN. RNR有机嵌段异质结构, 由于其逐渐掺杂的异质结而表现出渐变色的发射和波导特性, 而NRN有机嵌段异质结构由于其明显的构筑异质结界限而表现出纯双色发射和波导特性. 本工作实现了有机嵌段异质结构中嵌段块的有序可控生长, 为未来光子学发展提供了制备合理复杂有机嵌段异质结构的途径.

